Paper

THE SENSITIVITY OF ATMOSPHERIC DISPERSION CALCULATIONS IN NEAR-FIELD APPLICATIONS: MODELING OF THE FULL SCALE RDD EXPERIMENTS WITH OPERATIONAL MODELS IN CANADA, PART I

Luke Lebel,† Pierre Bourgouin,§ Sohan Chouhan,† Nils Ek,§ Volodymyr Korolevych,† Alain Malo,§ Dov Bensimon,§ and Lorne Erhardt*

Abstract—**Three radiological dispersal devices were detonated in 2012 under controlled conditions at Defence Research and Development Canada's Experimental Proving Grounds in Suffield, Alberta. Each device comprised a 35-GBq source of ^{140}La. The dataset obtained is used in this study to assess the MLCD, ADDAM, and RIMPUFF atmospheric dispersion models. As part one of a two-part study, this paper focuses on examining the capabilities of the above three models and evaluating how well their predictions of air concentration and ground deposition match observations from the full-scale RDD experiments.**
Health Phys. 110(5):499–517; 2016

Key words: contamination, environmental; emergencies, radiological; modeling, environmental; modeling, meteorological

INTRODUCTION

THE *FULL Scale Radiological Dispersal Device (RDD) Experiments* were carried out in 2012 at Defence Research and Development Canada's Experimental Proving Grounds in Suffield, Alberta (Green et al. 2016). Three integrated RDD experiments were conducted as part of the test series with the aim of characterizing how radiological material spreads through the air following the deployment of a real, full-scale weapon. The tests each involved explosively dispersing about a 35 GBq source of ^{140}La, and as the radioactive clouds that were produced spread out over the surrounding area, an array of different instruments tracked how contamination dispersed and settled over the nearby grassland. The wealth of information that was obtained now provides an extremely valuable dataset with which different public safety-oriented atmospheric dispersion models that are employed in Canada can be assessed.

The study presented here follows up on these trials and investigates the ability of three different atmospheric dispersion models [namely, *Modèle Lagrangien à Courte Distance* (MLCD; Flesch et al. 2002), Atmospheric Dispersion and Dose Analysis Method (ADDAM; Scheier 2009), and Risø Mesoscale Puff model (RIMPUFF; Thykier-Nielsen et al. 1999)] to reproduce the experimental data. The three models use fundamentally different calculation techniques to evaluate dispersion, employing Lagrangian particle, Gaussian plume, and Lagrangian puff formulations, respectively.

The area of highest concern, in terms of the public safety consequences of a radiological dispersal device, would likely be at length scales on the order of 500 m or less (Harper et al. 2007). Locally, contamination levels could still be quite high, but compared to other safety applications in which atmospheric dispersion models might be applied, like industrial emissions, large chemical fires, nuclear accidents, etc., the overall extent of contamination would be much smaller. Atmospheric dispersion models and the submodels that they contain are typically meant to examine dispersion over these much larger length scales, on the order of tens to hundreds of kilometers.

For MCLD, ADDAM/CSA-ERM, and RIMPUFF, therefore, this study intends to examine the lower bound for which these currently deployed operational models might be applicable. In doing so, important near-field dispersion modeling considerations will be identified, and the performance of these well established models in modeling RDD events will be examined. Most importantly, the information provided by the DRDC Suffield Full Scale RDD Experiments provides an opportunity to validate many aspects of each of these models against data collected from a very unique type of event.

*Defence Research and Developmet Canada, Ottawa Research Centre, Ottawa, Ontario, Canada; †Canadian Nuclear Laboratories, Chalk River, Ontario, Canada; §Environment Canada, Canadian Meteorological Centre, Dorval Quebec, Canada.

The authors declare no conflicts of interest.

For correspondence contact: Canadian Nuclear Laboratories, Chalk River, Ontario, Canada, or email at **luke.lebel@cnl.ca**.

(*Manuscript accepted* 3 *August* 2015)
0017-9078/16/0

DOI: 10.1097/HP.0000000000000365

Table 1. Physical measurements used in model comparison (Korpach et al. 2016; Erhardt et al. 2016).

Metric	Measurement	Units
Cloud integrated air concentration	High volume air samplers run continuously. Total activity on filters analyzed with high purity germanium detector.	Bq m^{-3}
Ground deposition concentration	Witness plate array, measurements with handheld AB100 taken 1 cm from surface.	Bq m^{-2}
Cloud shine dose	RadEye detector array, integrated dose of plume passage.	μGy
Ground shine dose rate	RadEye detector array, average dose rate immediately following plume passage.	μGy h^{-1}

This study is presented in two parts. This paper is Part I, which provides detail about the models themselves and evaluates how the predicted air concentrations and ground depositions compare against measurements. Model predictions in this paper are presented as a sensitivity study, evaluating: (i) meteorology, (ii) release height information, and (iii) particle size characterization influence predictions. The relative importance of each of these input factors in achieving reasonable predictions is evaluated to determine which factor would be the most important to ensuring accurate predictions for emergency planning or response. Part II of this study, which is presented in Lebel et al. (2016), evaluates how the concentration predictions made by the atmospheric dispersion models are converted to a radiation dose rate and how those predictions compare to the field measurements.

AVAILABLE MEASUREMENTS AND INPUTS

There were many independent measurement techniques that were employed to track aspects of the dispersion, deposition, and dose rates resulting from the RDD releases. Those assessed against the dispersion model predictions in Part I and Part II of this study were those taken from fixed arrays of detectors for quantifying the ground deposition (Erhardt et al. 2016), the radiation from the plume passage (Korpach et al. 2016), and the air concentrations (Okada et al. 2016). An overview of all of these, as well as other tools to monitor weather conditions and a discussion of important operational aspects of the trials, is given in Green et al. (2016).

The four aspects that are most important to atmospheric dispersion modeling, however, are: (i) the integrated air concentration of the passing plume, (ii) total cloud shine dose from the passing plume, (iii) the ground concentration of deposited radioactive material, and (iv) the ground shine dose rate from deposited material. Integrated air concentration and cloud shine are important for characterizing the short term exposure to an RDD event, while ground deposition and ground shine are each important in characterizing the overall long term contamination and how much cleanup effort is subsequently required.

Fixed-point measurements have a clear source-receptor relationship, and as such, they can be used easily as a basis for comparison between measurements and the atmospheric dispersion model predictions. This paper (Part I of this study) focuses on dispersion within 500 m of the source and compares results to the air samplers and witness plate beta deposition measurements. Part II of this study (Lebel et al. 2016) focuses more on the radiation and dose aspects of atmospheric dispersion modeling and compares results to the RadEye radiation monitor array measurements. These physical measurements are each described in Table 1.

Airborne and deposited radioactivity measurements

The three RDD tests are discussed in this section. In each test, when the RDD was detonated, a radioactive cloud containing the ^{140}La radionuclide was formed. As the clouds spread downwind, high volume air sampling instruments, run by personnel from the U.S. Department of Energy Remote Sensing Laboratory (RSL), captured material as it traveled overhead, collecting it on a filter and employing a high purity germanium gamma spectrometer to quantify the integrated concentration to which the air sampler was exposed (Okada et al. 2016). The air samplers reported data at 10 and 13 different locations during shot 1 and shot 2, respectively, and were not deployed during shot 3. A map of the measurement results and profiles along the approximate plume centerline are shown in Fig. 1. Results are reported as dilution ratios, φ, which are the integrated concentration values, $\langle c_{air}t\rangle$, normalized by the initial source activity, Q:

$$\chi = \frac{1}{Q}\int c_{air}dt = \frac{\langle c_{air}t\rangle}{Q}. \quad (1)$$

Dispersed material from the RDDs also deposited on the ground after each shot, including on a series of 0.1 m × 0.1 m aluminum witness plates. The radioactivity on each witness plate was measured using a portable AB100 beta radiation detector, allowing the local ground contamination at each of the >300 field locations to be measured (Erhardt et al. 2016). Contour plots of the ground contamination following each shot, as well as the contamination along the approximate plume centerlines, are shown in Fig. 2. Again,

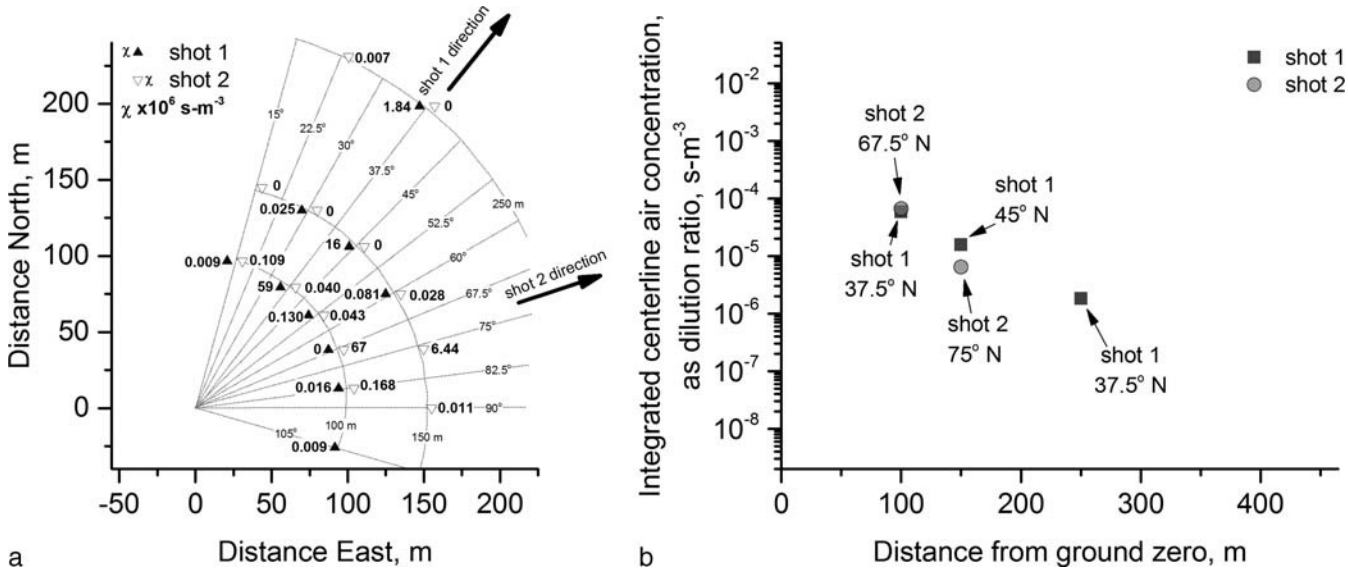

Fig. 1. Integrated air concentration profiles, as dilution ratios, from RSL high volume air sampler measurements (Okada et al. 2016): (a) measurement map; (b) centerline measurements.

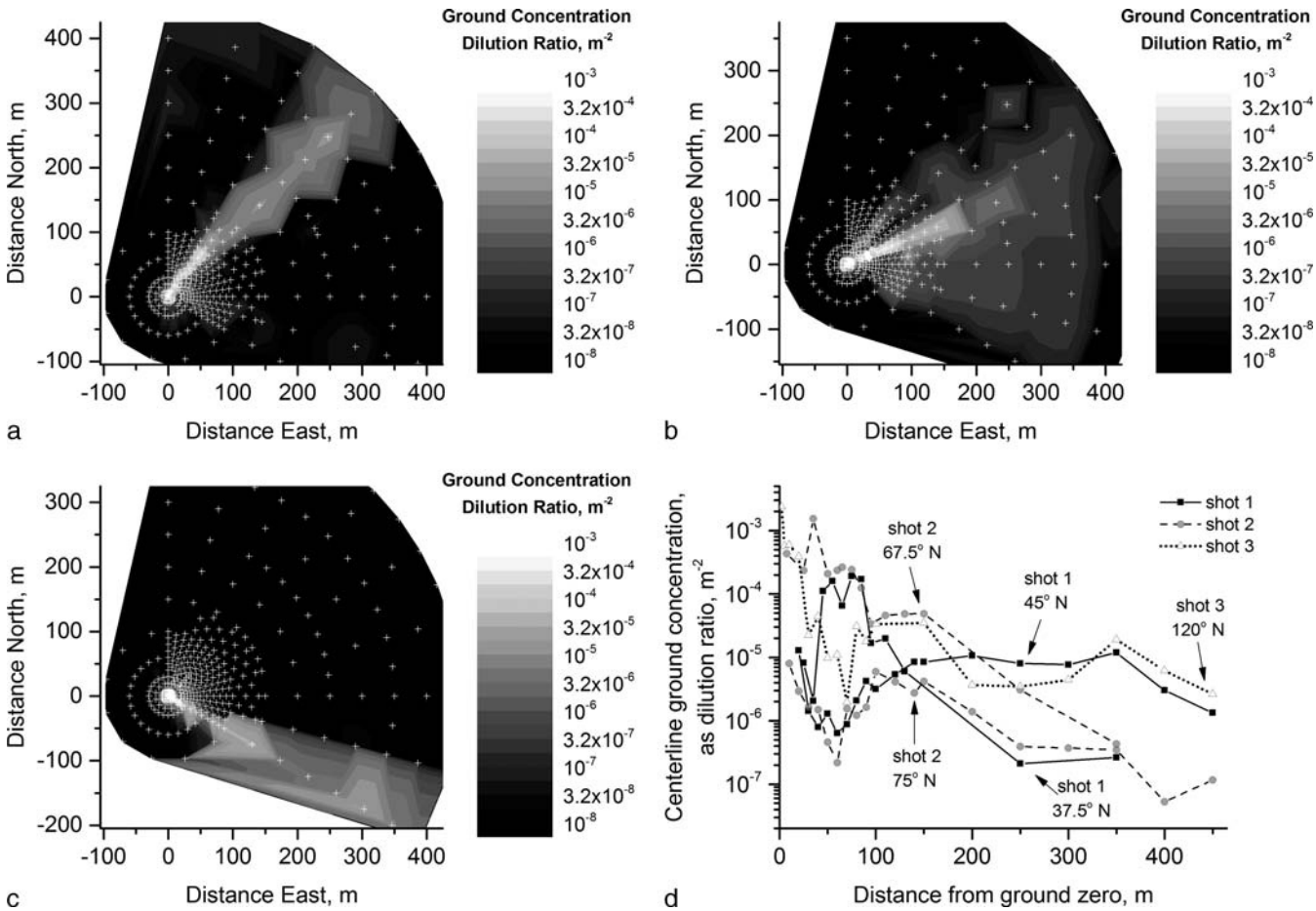

Fig. 2. Ground deposition profiles, as dilution ratios, from witness plate deposition measurements (Erhardt et al. 2016): (a) shot 1 measurement map; (b) shot 2 measurement map; (c) shot 3 measurement map; (d) centerline measurements.

results are reported as dilution ratios, ω, which are the absolute ground deposition values, c_{dep}, normalized to the initial source activity, Q:

$$\omega = \frac{c_{dep}}{Q}. \quad (2)$$

It is clear in Fig. 2a–c that the plume centerlines, as marked by the highest ground concentrations, were between 37.5° N and 45° N for shot 1, between 67.5° N and 75° N for shot 2, and around 120° N for shot 3. The contour plot in Fig. 2c may be slightly distorted because the plume in shot 3 traveled near the edge of the fixed-point detector array. For shot 1 and 2, because the plume passed in between two detector azimuth lines, measurements from both adjacent lines are given in the centerline plot in Fig. 2d.

Meteorological measurements

There were several different meteorological stations deployed at various locations during the RDD trials, including a set of three sonic anemometers mounted on a tower at a short distance southwest of ground zero. The anemometers were mounted at 2 m, 4.5 m, and either 12 m (for shots 1 and 2) or 10 m (for shot 3) above ground. These anemometer measurements have been selected to be used as input data for the modeling work in this study because of their close proximity to the shot, time resolution, and detailed information about the 3-dimensional properties of the local winds. Likewise, the measurements taken at the highest point on the tower, 12 m or 10 m as applicable, were considered most appropriate as inputs for the dispersion models.

The sonic anemometer measurements have been employed to obtain different statistics about the wind conditions in the local environment. Important among these are the wind speed, $\bar{u}$; horizontal wind direction, θ; and vertical wind direction, ϕ. The variability in the wind speed and direction reported by the sonic anemometers are also important model inputs. Each mean meteorological parameter has a corresponding standard deviation, σ_u, σ_θ, and σ_ϕ, which is employed in each of the atmospheric dispersion models to evaluate dispersion parameters. MLCD, ADDAM/CSA-ERM, and RIMPUFF each evaluated dispersion statistics over a 10-min time window, and the meteorological inputs for each of these models, accordingly, were presented in Green et al. (2016) and are given in Table 2.

Table 2. Mean and standard deviation of meteorological inputs, $\bar{u} \pm \sigma_u$, $\theta \pm \sigma_\theta$, and $\phi \pm \sigma_\phi$, from sonic anemometer measurements (from Green et al. 2016).

	Shot 1	Shot 2	Shot 3
Wind speed, ms^{-1}	7.98 ± 1.24	4.45 ± 0.69	2.92 ± 0.56
Horizontal direction, deg	226.2 ± 5.9	261.7 ± 12.0	298.4 ± 10.8
Vertical direction, deg	2.40 ± 2.89	0.89 ± 4.68	0.89 ± 5.88
Stability class	E	E	D

Source term particle size distribution and deposition velocity

The sizes of radioactive particles emitted by radiological dispersal devices have a major influence over their overall dispersion, since the deposition velocity of a particle is so closely linked to its size. Large particles, for example, which settle out of the air much faster, would be deposited in high concentrations close to the source. Small particles, on the other hand, can stay suspended in the air for much longer, and thus contamination would generally be more diffuse but also much more widespread.

Studies that attempted to characterize the particle size distribution of dispersed material were carried out in the lead-up to the full scale tests in 2012. At the Royal Military College of Canada (Lebel et al. 2012; Lebel 2012), small scale tests were carried out in a closed vessel with charges about one-tenth the size of the full scale charges. Residual materials were collected from the closed vessels and found with a laser diffraction particle sizing system to have a mass median particle size of about 45 μm. Control samples of the original La_2O_3 powder were also analyzed in this way and found to have a mass median particle size of about 25 μm. According to the study, the growth in particle size was likely due to agglomeration of the La_2O_3 particles with themselves, as well as with carbonaceous soot and other materials entrained in the fireball. Further tests on a full-scale device carried out at the explosive test facility at Sandia National Laboratories were in fair agreement with these measurements (Green et al. 2016).

ATMOSPHERIC DISPERSION MODELS

Three operational atmospheric dispersion models are being employed in this study to model the releases from the DRDC Suffield full-scale RDD trials. MLCD, ADDAM, and RIMPUFF employ fundamentally different underlying models and are used for different purposes by organizations and governments in Canada and around the world.

The capabilities and modeling parameters for the three models are compared in Table 3, and although, by and large, they have similar capacities, none have been designed to model the dispersion from an RDD. The near-field nature of the problem poses a challenge for each of these models, and the purpose of this study is to evaluate how well they would be able to model such events if required. Just as importantly, since in a real situation it could be difficult to obtain reliable information sufficient to fill in all of the necessary inputs, effort will be made to evaluate which input parameters are the most important in obtaining the

Table 3. Capabilities and set up of the MLCD (Flesch et al. 2002), ADDAM/CSA-ERM (Scheier 2009), and RIMPUFF (Thykier-Nielsen et al. 1999) atmospheric dispersion models.

	MLCD	ADDAM/CSA-ERM	RIMPUFF
Dispersion	Lagrangian particle dispersion model, calculates trajectories of individual air parcels and their dispersion from turbulent fluctuations of the wind. Trajectories calculated based on velocity increments, based on Langevin Stochastic Equation and atmospheric turbulence kinetic energy (Flesch et al. 2002). Turbulence parameters are based on stability class and terrain type.	Gaussian plume model, employing lateral and vertical dispersion coefficients, σ_y and σ_z, as defined in CSA N288.2-M91 standard (CSA 1991). Coefficient σ_y is defined based on average wind fluctuations, σ_θ, while coefficient σ_z is based on the vertical Pasquill stability class.	Lagrangian puff model is a superposition, over time, of Gaussian puffs. The lateral, and vertical dispersion coefficients, σ_y and σ_z, are calculated based on stability classes derived from average wind speeds, time of day, and season (Kerschgens and Suer 1988).
Spatial grid	Calculates output parameters at any receptor location within a user-defined computational grid domain. A spatial resolution (grid mesh) of ~7 m was used in this study (1.7 km × 1.7 km domain).	Calculates output parameters at receptor locations ±30° of mean wind, and beyond 40 m from source (modified from 100 m minimum in developmental version).	A minimum grid size of 50 m by 50 m is available, and concentrations are averaged within each grid cell.
Time resolution	A time resolution of 5 s was employed in this study	The minimum time resolution of 10 min was employed in this study.	A time resolution of 10 s was employed in this study (modified from 60-s minimum in developmental version).
Release	Particles are distributed uniformly and randomly in the vertical in a fixed cylinder of a specific predefined height (no buoyancy or momentum).	Model has plume buoyancy and momentum capability, but non-buoyant release height and cloud shape were manually set for this study.	Model has plume buoyancy and momentum capability, but non-buoyant release height and cloud shape were manually set for this study.
Deposition	Uses particle reflection probability, based on user-defined deposition velocity, v_d, for dry deposition (Wilson et al. 1989). Wet deposition not employed in this study.	Uses user-defined deposition velocity, v_d, to handle dry deposition. Wet deposition not employed in this study.	Dry deposition velocity, v_d, determined based on surface type only. Wet deposition not employed in this study.
Radioactivity	Handles single-nuclide radioactive decay.	Handles radioactive decay and build-up for multiple radionuclides.	Handles radioactive decay and build-up for multiple radionuclides.

most reasonable best estimates for radionuclide dispersion and deposition.

MLCD

MLCD is an operational atmospheric dispersion model and emergency response tool that is used by Environment Canada to predict the spread of pollutants or hazardous materials. It has two sister models, *Modèle Lagrangien de Dispersion de Particules d'ordre 0* and *d'ordre 1*, MLDP0 and MLDP1 (D'Amours et al. 2015), that operate similarly, but MLCD is designed specifically to evaluate dispersion over short ranges (<10 km from the source). MLCD is a first order Lagrangian particle dispersion model whereby the 3-D trajectories of a very large number of air particles are calculated, employing the Langevin stochastic equation based on turbulent fluctuations in the wind (Flesch et al. 2002). These fluctuations, in turn, can be obtained from real meteorological tower observations, as well as real-time forecasts from a numerical weather prediction system.

The principle behind the first order Lagrangian stochastic particle model in MLCD is that the position, x_i, and velocity, u_i, of, thousands of individual particles are tracked, and the velocity is the sum of the average Eulerian component, the stochastic fluctuation and the mesoscale fluctuation, $u_i = U_i + u_i' + u_i^m$. The change in particle position over a small increment of time, dt, is given by:

$$dx_i = u_i dt, \tag{3}$$

and the change in the stochastic component of particle, $\boldsymbol{u_i'}$, velocity is calculated with a generalized Langevin equation:

$$du_i' = a_i dt + b_{ij} d\xi_j \tag{4}$$

where:

$\boldsymbol{x_i}$ = the position vector of particle i;

$\boldsymbol{u_i}$ = the velocity vector of particle i;

$\boldsymbol{U_i'}$ = the vector of the average wind velocity of particle i;

$\boldsymbol{u_i'}$ = the vector of the stochastic fluctuation velocity of particle i;

$\boldsymbol{u_i^m}$ = the horizontal vector of mesoscale velocity of particle i;

$\boldsymbol{a_i}$, $\boldsymbol{b_{ij}}$ = Langevin equation coefficients that depend on particle i velocity and position; and

$\boldsymbol{d\xi_j}$ = a vector of Gaussian random numbers with zero average and variance dt.

In MLCD, a realistic vertical wind profile of $\boldsymbol{U_i}$ and other parameters describing the boundary layer (friction velocity, Monin-Obukhov length, boundary layer height) are calculated through an analytical average wind model (Wilson and Flesch 2004).

ADDAM/CSA-ERM

ADDAM is a Canadian nuclear safety model that employs a Gaussian plume model to predict the dispersion of radiological materials emitted from a reactor accident (Scheier 2009). It is used by the Canadian Nuclear Safety Commission and the Canadian nuclear industry to quantify the radiological dose that individuals exposed to the plume might obtain, as well as the air concentrations and ground deposition that could be expected over the course of an accident. ADDAM is designed to adhere to classical plume modeling techniques in accordance with a national Canadian nuclear safety standard, CSA N288.2-M91 (CSA 1991). The basic premise of the model is to be able to predict the public dose consequences of a radiological release, as would be required for emergency planning and nuclear safety analysis.

The Gaussian plume model contained within ADDAM employs the following expression, where the dilution ratio, $\chi = c_{air}/Q$, is governed by:

$$\chi = \frac{1}{2\pi\bar{u}\sigma_y\sigma_z}\exp\left(-\frac{y^2}{2\sigma_y^2}\right)$$

$$\left[\exp\left(-\frac{(z-H)^2}{2\sigma_z^2}\right) + \exp\left(-\frac{(z+H)^2}{2\sigma_z^2}\right)\right]f_c, \qquad (5)$$

where:

x,y,z = downwind, crosswind, and vertical position with respect to release point;

$\bar{u}$ = mean wind velocity;

σ_y, σ_z = horizontal and vertical dispersion coefficients;

H = release height; and

f_c = capping inversion correction factor.

ADDAM is governed by strict quality assurance and version control guidelines according to the CSA standard. In this study, a developmental version of ADDAM, CSA-ERM (Canadian Standards Association–Emergency Response Model) was employed in order to modify different input and output parameters and remove restrictions in order to allow this model to make predictions in the very near-field, within 100 m.

RIMPUFF

RIMPUFF, Risø Mesoscale Puff model, is a European dispersion model employed to estimate the consequences of a release of hazardous materials into the atmosphere (Thykier-Nielsen et al. 1999). It is the dispersion engine incorporated into the RODOS (Real-time On-line DecisiOn Support; Ehrhardt and Weis 2000) and ARGOS (Accident Reporting and Guidance Operational System; Hoe et al. 2009) accident consequence analysis and support system, which are employed by Health Canada and other governmental organizations in Canada as well as different national authorities throughout the world. RIMPUFF was designed to support decision making in the wake of a nuclear accident, and like ADDAM/CSA-ERM, it has the capability to evaluate radiological dose and possible health consequences; it is equally qualified to model the dispersion of any material, hazardous or otherwise, in the atmosphere. One of the unique aspects of this model is that it is a hybrid between the Lagrangian particle dispersion technique and the classical Gaussian plume models. By superimposing different Gaussian plumes, RIMPUFF has the capability to better handle inhomogeneity in atmospheric turbulence and weather conditions and changes in conditions over time, while still retaining much of the simplicity of classical models.

The dilution ratio, χ_i, of each individual puff at a particular point in time is governed by the following expression, and then RIMPUFF calculates the superimposition of each to determine the total dilution ratio of a release:

$$\chi_i = \frac{1}{(2\pi)^{3/2}\sigma_{x,i}\sigma_{y,i}\sigma_{z,i}}\exp\left(-\frac{(x-x_{c,i})^2}{2\sigma_{x,i}^2} - \frac{(y-y_{c,i})^2}{2\sigma_{y,i}^2}\right)$$

$$\left[\exp\left(-\frac{(z-z_{c,i})^2}{2\sigma_{z,i}^2}\right) + \exp\left(-\frac{(2z_{inv}-z_{c,i})^2}{2\sigma_{z,i}^2}\right)\right], \qquad (6)$$

where:

x,y,z = downwind, crosswind, and vertical position with respect to the center of puff i;

$x_{c,i}, y_{c,i}, z_{c,i}$ = downwind, crosswind, and vertical position of the center of puff i with respect to the release point;

z_{inv} = height of a capping inversion with respect to the center of puff i; and

$\sigma_{x,i}, \sigma_{y,i}, \sigma_{z,i}$ = downwind, horizontal, and vertical dispersion coefficients for puff i.

MODELING PARAMETERS

Meteorological parameters

Meteorological parameters include the wind speed, direction, and variability. In classical atmospheric dispersion based on statistical diffusion theory (Taylor 1921), the lateral and vertical dispersion coefficients, σ_y and σ_z, are typically proportional to the horizontal and vertical wind fluctuations, σ_θ and σ_ϕ, and increase with distance from the source based on the time scales of the atmospheric turbulence and wind speed (Arya 1999):

$$\sigma_y = \sigma_\theta x f_y\left(\frac{x}{\bar{u}T_L}\right) \tag{7}$$

$$\sigma_z = \sigma_\phi x f_z\left(\frac{x}{\bar{u}T_L}\right), \tag{8}$$

where x is the distance downwind, and T_L is the Lagrangian time scale of the atmospheric turbulence. There are a number of different formulations for $(x \times f_y)$ and $(x \times f_z)$ in the literature, but generally they increase monotonically with distance and often in a power law relationship with distance.

As a statistical theory, classical turbulent diffusion theory is not intended to describe the dispersion of a particular parcel of gas or describe the shape of a contaminant cloud at a given instance in time. Rather, it describes a probability or a shape that a cloud might take if it is taken as the ensemble average of many individual releases. However, the statistical theory does give the general trend of how dispersion behaves. For example, higher degrees of instability in the atmosphere and larger fluctuations in the wind would result in faster dispersion, meaning slightly lower plume centerline concentrations and more lateral dispersion. Stronger, less fluctuating winds, on the contrary, would result in narrower plumes and contamination clouds being carried downwind more quickly. Each of the dispersion models described below incorporates statistical diffusion theory in their calculations, and either uses the analytical solutions that are derived from it or attempts to model the stochastic nature of atmospheric dispersion directly.

MLCD uses this latter approach, employing the Langevin expression described in eqn (4). The coefficients of this expression, $\boldsymbol{a_i}$ and $\boldsymbol{b_{ij}}$, contain information about meteorological parameters and turbulence, where:

$$a_u = -\frac{C_o\epsilon}{2\sigma_u^2}u' + \frac{1}{2\sigma_u^2}\frac{\partial\sigma_u^2}{\partial z}u'w' \tag{9}$$

$$a_v = -\frac{C_o\epsilon}{2\sigma_v^2}u' + \frac{1}{2\sigma_v^2}\frac{\partial\sigma_v^2}{\partial z}v'w' \tag{10}$$

$$a_w = -\frac{C_o\epsilon}{2\sigma_w^2}w' + \frac{1}{2}\frac{\partial\sigma_w^2}{\partial z}\left(\frac{w'^2}{\sigma_w^2}+1\right) \tag{11}$$

$$b_u = b_v = b_w = \sqrt{C_o\epsilon}, \tag{12}$$

where:

$\sigma_u^2, \sigma_v^2, \sigma_w^2$ = Eulerian velocity variances in the x, y, and z direction;

u', v', w' = wind velocity fluctuations in the x, y, and z direction;

$u'w'$, $v'w'$, w'^2 = covariance between the vertical and x, y, and z direction wind velocity fluctuations;

C_o = a constant assumed to be equal to 3.0; and

ε = turbulent kinetic energy dissipation rate.

MLCD contains parameterizations that relate the velocity variances, σ_x^2, σ_y^2, and σ_z^2, and turbulent kinetic energy dissipation rate, ε, to the atmospheric friction velocity, u_* and boundary layer height, h. The parameterizations follow those of Rodean (1996) and assume that the two horizontal variance components are equal. For stable or neutral atmospheric conditions, this is:

$$\sigma_u^2 = \sigma_v^2 = u_*^2\left[4.5\left(1-\frac{z}{h}\right)^{1.5}\right] \tag{13}$$

$$\sigma_w^2 = u_*^2\left[2\left(1-\frac{z}{h}\right)^{1.5}\right] \tag{14}$$

$$\epsilon = \frac{u_*^3}{kz}\left(1+3.7\frac{z}{h}\right)\left(1-0.85\frac{z}{h}\right)^{1.5}, \tag{15}$$

where $k = 0.4$ is von Karman's constant. In general, MLCD sets h = 300 m for stable conditions and h = 1,000 m for neutral conditions. Using data from wind measurements, in this case from the sonic anemometer, the model employs an optimization routine to calculate the friction velocity, u_*. With the friction velocity known, the turbulence and dispersion parameters can be calculated directly.

ADDAM/CSA-ERM also has the capability to incorporate meteorological measurement in its calculations. The lateral dispersion coefficient, σ_y, is calculated as a function of downwind distance using the standard deviation of horizontal wind measurements, σ_θ, employing the following expression from Hanna et al. (1977) for dispersion within 10 km:

Table 4. Stability-dependent parameters for the ADDAM/CSA-ERM vertical dispersion coefficient (Scheier 2009).

Pasquill stability class	a_1	b_1	a_2	b_2
A	0.112	1.060	5.38×10^{-4}	0.815
B	0.130	0.950	6.52×10^{-4}	0.750
C	0.112	0.920	9.05×10^{-4}	0.718
D	0.098	0.889	1.35×10^{-3}	0.688
E	0.0609	0.895	1.96×10^{-3}	0.684
F	0.0638	0.783	1.36×10^{-3}	0.672

$$\sigma_y = \sigma_\theta \frac{x}{1 + 0.0406x^{0.423}}. \tag{16}$$

The value of the vertical dispersion coefficient, σ_z, as a function of distance, however, is only based on stability category and surface roughness, where:

$$\sigma_z = \frac{a_1 x^{b_1}}{1 + a_2 x^{b_2}} \times \ln\left(\frac{c_1 x^{d_1}}{1 + c_2 x^{d_2}}\right). \tag{17}$$

The parameters in this expression are available in Table 4 and Table 5.

RIMPUFF, with its hybrid method, correlates its dispersion coefficients as a function of time after release to the standard deviation of wind fluctuations, σ_u, σ_v, and σ_w, as well as the Lagrangian time scales of atmospheric turbulence in each respective dimension, $T_{L,u}$, $T_{L,v}$, and $T_{L,w}$:

$$\sigma_x = \frac{\sigma_u t}{\sqrt{1 + \frac{t}{2T_{L,u}}}}, \ \sigma_y = \frac{\sigma_v t}{\sqrt{1 + \frac{t}{2T_{L,v}}}},$$

$$\sigma_z = \frac{\sigma_w t}{\sqrt{1 + \frac{t}{2T_{L,w}}}}. \tag{18}$$

These parameters, based on Kerschgens and Suer (1988), can be calculated based on the atmospheric friction velocity (u_*), convective velocity scale (w_*), and height of the mixed layer (h_m) for different atmospheric conditions. Instead of using direct measurements, however, RIMPUFF uses these parameterizations, which in turn are based on atmospheric stability:

$$\sigma_u = \left[(2.4u_*)^3 + (0.60w_*)^3\right]^{1/3} \text{(unstable/neutral)}, \ \sigma_u = 2.4u_* \text{ (stable)} \tag{19}$$

$$\sigma_v = \left[(1.8u_*)^3 + (0.56w_*)^3\right]^{1/3} \text{(unstable/neutral)}, \ \sigma_v = 1.8u_* \text{ (stable)} \tag{20}$$

$$\sigma_w = \left[(1.3u_*)^3 + (0.56w_*)^3\right]^{1/3} \text{(unstable/neutral)}, \ \sigma_w = 1.3u_* \text{ (stable)} \tag{21}$$

$$T_{L,u} = 0.15\frac{h_m}{\sigma_u} \text{ (unstable/neutral/stable)} \tag{22}$$

$$T_{L,v} = T_{L,w} = 0.15\frac{h_m}{\sigma_u} \text{ (unstable/neutral)}, \ T_{L,v} = T_{L,w} = 0.10\frac{h_m}{\sigma_u} \text{ (stable)}. \tag{23}$$

Release height

The cloud from a high explosive detonation immediately begins to rise into the air due to buoyancy as a result of the amount of heat energy given off by the explosion. The explosive charges were initiated 1 m above the ground during the Full Scale RDD tests, and as seen in the video frames in Fig. 3, a cloud rise of several meters in a few seconds can be seen.

Since the vertical plume centerline would be higher above ground level, what this buoyant rise serves to do effectively is to increase the distance between the bulk of the airborne contamination and the ground. In a classic Gaussian model of dispersion, ground level concentration is related to the effective release height by $exp\left(-{}^1/_2 H^2/\sigma_z^2\right)$. The relationship is not particularly strong when $H << \sigma_z$ at receptor locations far from the source. On the other hand, when $H >> \sigma_z$ at receptor locations near the source with elevated or very buoyant releases, release height would have a very strong influence in decreasing ground level concentration.

Cao et al. (2011) developed an empirical cloud rise model based on numerous small explosive charges in the 0.025- to 5-kg size range, using cloud-mapping measurements to track the buoyant rise of emissions within the first 2 min after detonation. They developed a simple relationship that predicts the cloud top height, h (in meters), reasonably well and based only on time after detonation, t (in seconds), and the weight of the charge, w (in kg):

$$h(w, t) = 7.4w^{0.18}t^{0.55}. \tag{24}$$

Based on the 208 g charges employed in the Full Scale RDD trials, this would predict a cloud top height between 8 and 14 m high in the first 2-5 s after the detonation. This is reasonably consistent with the images shown of shot 2 in Fig. 3. After about the first 5 s, the buoyant rise for the amount of energy emitted in these

Table 5. Roughness-dependent parameters for the ADDAM/CSA-ERM vertical dispersion coefficient (Scheier 2009).

Roughness length, m	c_1	d_1	c_2	d_2
0.01 e.g., water	1.56	0.048	6.25×10^{-4}	0.45
0.04 e.g., plowed land	2.02	0.0269	7.76×10^{-4}	0.37
0.1 e.g., grassland	2.72	0	0	0

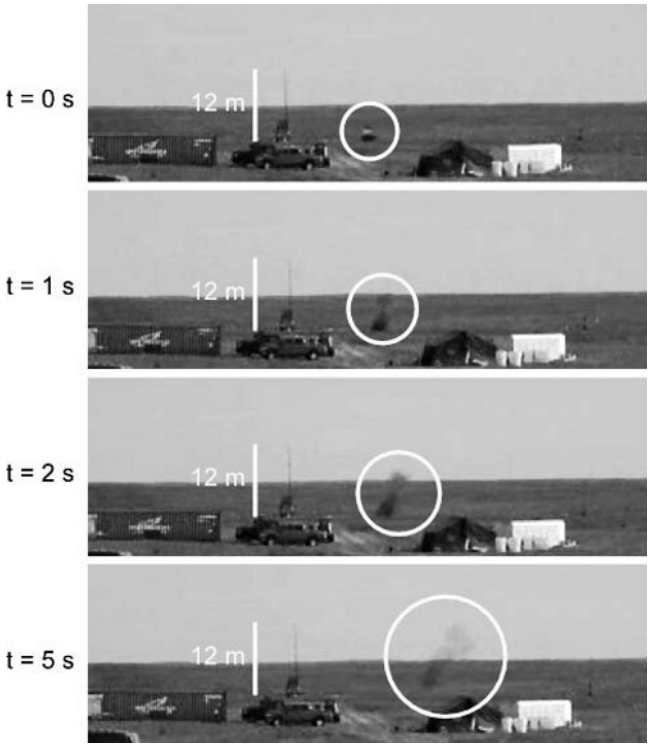

Fig. 3. Sequence showing cloud rise during shot 2 of the Full Scale RDD trials.

cases would become less important than normal vertical dispersion.

Since the models being compared in this study do not necessarily contain buoyant cloud rise models (and if they do, they are designed more for smokestacks, fires, and other continuous emission sources), buoyant rise in this study is being handled artificially, based on judgments made from videos of the detonations and the Cao et al. (2011) model. For MLCD, the initial cloud could be defined as a cylinder with a defined height and radius in which the Lagrangian particles are randomly distributed. The only practical means in RIMPUFF to simulate the cloud rise following the explosion is to increase the release height; it can only treat the release as an elevated point source, however.

In ADDAM/CSA-ERM, releases are normally treated as point sources as well. The model, however, contains a model that can be used to artificially increase the initial size of the cloud at the source. It was originally developed and implemented in ADDAM as a correction for building wake effects, but it is mathematically identical to a situation where the cloud has an initial size at the time of the release:

$$\sigma_{y*} = \sqrt{\sigma_y^2 + \frac{C_b A_b}{\pi}} \tag{25}$$

$$\sigma_{z*} = \sqrt{\sigma_z^2 + \frac{C_b A_b}{\pi}}. \tag{26}$$

where σ_{y*} and σ_{z*} are the corrected lateral and vertical dispersion parameters, A_b is the building area or cloud area parameter, and C_b is a parameter with a value between 0.5 and 2.0. The term $C_b A_b/\pi$ is set to match the initial cloud sizes that were observed.

Deposition velocity

The flux of airborne material, F_c, toward the ground at any given point, for particles, is related to the ground level concentration, c, and the dry deposition velocity, v_d (Arya 1999):

$$F_c = v_d \overline{c}. \tag{27}$$

This relationship controls the amount of material that will be deposited on the ground as well as the depletion of contaminants in the cloud. The controlling term in eqn (27) is the dry deposition velocity, which effectively contains the transfer resistances that must be overcome to transport particles from the air and through any viscous sublayers until it can finally be deposited on a surface. Deposition mechanisms like Brownian diffusion can come into play for very fine particles, but for the particles being generated from these RDDs (Green et al. 2016), inertial impaction, and to an even greater extent gravitational settling, would likely be the most important mechanisms.

Green et al. (2016) and Lebel et al. (2012) each suggest that the distribution of particle sizes emitted from the RDDs deployed during the trials would be quite broad, with particles ranging from 10 μm in size to greater than 100 μm. Deposition is very strongly dependent on particle size, and the settling velocity due to gravity alone is proportional to the square of particle size. A one order of magnitude range in particle size, therefore, would translate into a two order of magnitude range in deposition velocities, according to Stokes' law:

$$v_d = \frac{\rho_p d_a^2 g}{18\mu_g} \text{ for Re} < 1.0, \tag{28}$$

where ρ_p and μ_g are the density of the particle and dynamic viscosity of air, respectively; g is the acceleration due to gravity; and d_a is the aerodynamic diameter of the particle (Hinds 1999). Whereas a 10-μm particle would only settle at 3.1 mm s^{-1} under the force of gravity, this would be 250 mm s^{-1} for a 100 μm particle. In evaluating the sensitivity of MLCD, ADDAM/CSA-ERM, and RIMPUFF to particle size, it is essential to evaluate these broad differences in deposition velocity and how they affect predictions. RIMPUFF and ADDAM/CSA-ERM each calculate the deposition profile using eqn (27).

MLCD, because of the way it uses Lagrangian particles in its calculations, defines a "reflection probability" (which is the probability, R) that a particle, according to

the stochastic calculations of its motion, impacts the ground, would reflect upward rather than be absorbed (Wilson et al. 1989). MLCD employs the ratio of deposition velocity and standard deviation of vertical wind velocity, v_d/σ_w:

$$R = \frac{1-\sqrt{\frac{\pi v_d}{2\sigma_w}}}{1+\sqrt{\frac{\pi v_d}{2\sigma_w}}}. \tag{29}$$

With the reflection probability defined, MLCD handles deposition by reducing the mass of each Lagrangian particle that impacts the ground, where M_o and M_1 are the pre- and post- impact particle mass. The Lagrangian particles or parcels in the MLCD simulations represent an ensemble of many real aerosol particles. The reduction in mass of the reflected Lagrangian parcel is meant to represent how some, but not all, of the real aerosol particles in the ensemble would deposit on the ground, while the remainder would stay suspended in the air:

$$M_1 = R\dot{c}M_o. \tag{30}$$

SENSITIVITY ANALYSIS

Taken altogether, each of these parameters—meteorological conditions, release characteristics, and deposition velocity—will all affect the dispersion and contamination profiles in different ways. The sensitivity of each can be evaluated, however, in order to show which will have the dominant effect on prediction results and which is most important to obtain the most accurate, best estimate results. The meteorological parameters for each shot, for example, were different, allowing predictions to be ranged between each of these. Likewise, two different release heights and two different deposition velocities were all evaluated. The different sensitivity parameters are tabulated in Table 6.

Cloud top heights of 10 m and 14 m, corresponding to 3-s and 5.5-s rise times in the Cao et al. (2011) model in eqn (24), were evaluated. The initial clouds extend from the ground to the cloud top height and to the centerline heights of the corresponding releases of 5 m and 7 m, respectively. Particles with aerodynamic diameters of 100 μm and 10 μm have deposition velocities of 250 mm s^{-1} and 3.1 mm s^{-1}, respectively, and each of these will be evaluated as well.

The flexibility of the RIMPUFF model was somewhat more limited, as a deposition velocity could not be specified explicitly. In addition, the release height was only modeled as a point source with a release height of 10 m. As such, only the sensitivity to wind and meteorological conditions are evaluated for RIMPUFF.

Sensitivity of integrated air concentration predictions

Integrated air concentrations, as dilution ratios, are shown for the three models in Figs. 4 to 6. The most concentrated regions of the plume are along its centerline, and as material travels downwind, it becomes more diffuse and dispersed.

For MLCD, integrated air concentration dilution ratios along the centerline are between about 10^{-3} s m^{-3} and 10^{-5} s m^{-3} in the 50 m to 400 m range downwind from the shot. The lateral dispersion predicted by MLCD is fairly insensitive to the different input parameters. Likewise, the downwind dispersion is fairly insensitive to release height and meteorological conditions. However, when a higher deposition velocity was set, the faster deposition rates meant that there was a larger degree of plume depletion, and concentrations downwind decreased faster.

With ADDAM/CSA-ERM, centerline integrated air concentration dilution ratios were again on the order of 10^{-3} s m^{-3} to 10^{-5} s m^{-3} within the first 500 m downwind and were fairly close to those predicted by MLCD. The lateral dispersion, however, was much more strongly influenced by meteorological conditions. When employing meteorological conditions from shot 1 in its calculations, where there was a very strong, direct wind, the lateral dispersion 100 m downwind was only about 60% as wide as when meteorological conditions from shot 2 or shot 3

Table 6. Parametric design for prediction sensitivity analysis.

	MLCD	ADDAM / CSA-ERM	RIMPUFF
Meteorological conditions			
shot 1 conditions	$\bar{u}$ = 8.0 ms^{-1}, σ_θ=5.9°	$\bar{u}$ = 8.0 ms^{-1}, σ_θ=5.9° stability E	$\bar{u}$ = 8.0 ms^{-1}, morning, summertime
shot 2 conditions	$\bar{u}$ = 4.5 ms^{-1}, σ_θ=12.0°	$\bar{u}$ = 4.5 ms^{-1}, σ_θ=12.0° stability E	$\bar{u}$ = 4.5 ms^{-1}, morning, summertime
shot 3 conditions	$\bar{u}$ = 2.9 ms^{-1}, σ_θ=10.8°	$\bar{u}$ = 2.9 ms^{-1}, σ_θ=10.8° stability D	$\bar{u}$ = 2.9 ms^{-1}, morning, autumn
Cloud top height			
	10 m	10 m	10 m
	14 m	14 m	
Deposition velocity			
	250 mms^{-1}	250 mms^{-1}	
	3.1 mms^{-1}	3.1 mms^{-1}	1 mms^{-1}

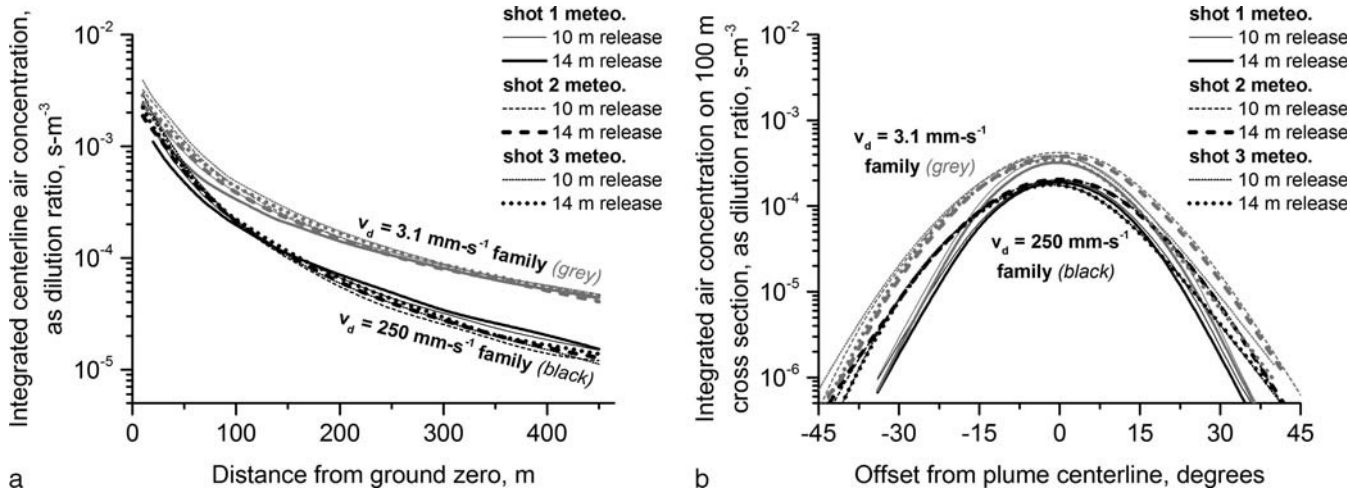

Fig. 4. Integrated air concentration profiles for MLCD, as dilution ratios: (a) centerline; (b) 100 m cross-section.

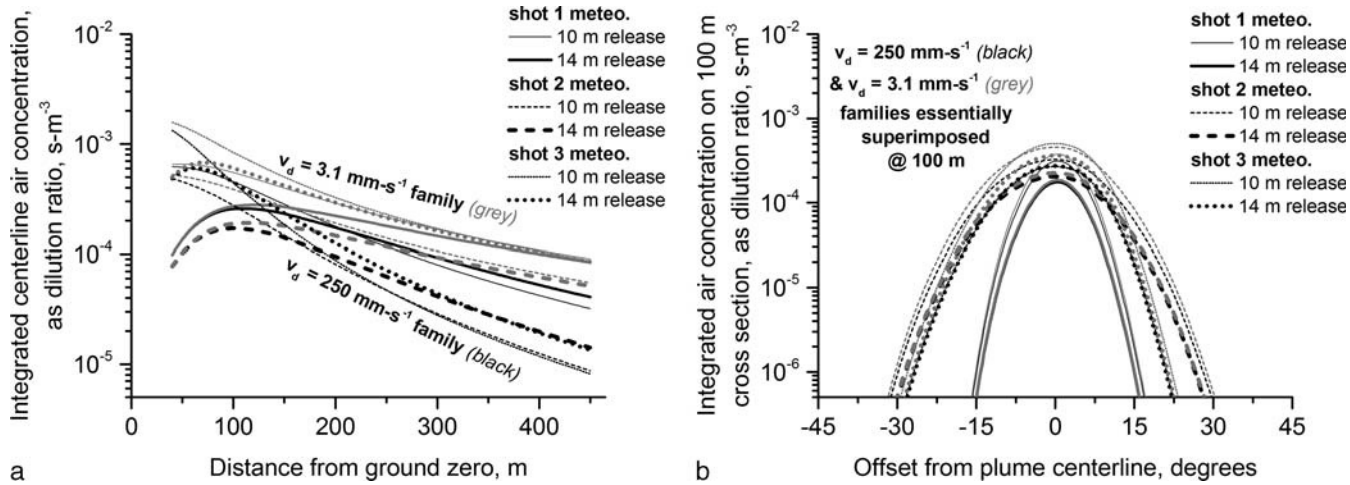

Fig. 5. Integrated air concentration profiles for ADDAM/CSA-ERM, as dilution ratios: (a) centerline; (b) 100 m cross-section.

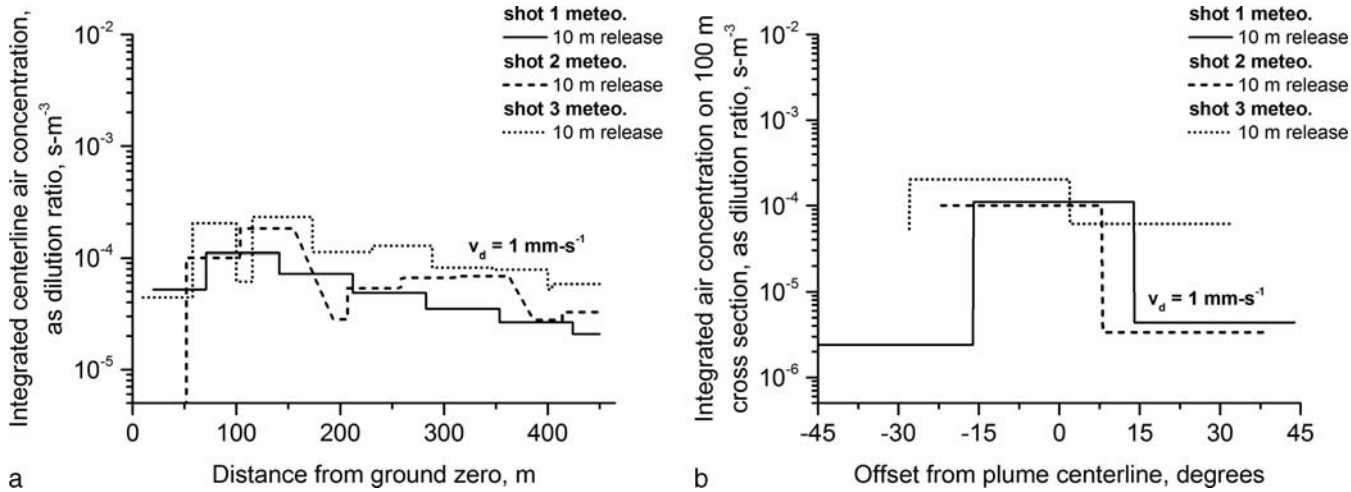

Fig. 6. Integrated air concentration profiles for RIMPUFF, as dilution ratios: (a) centerline; (b) 100 m cross-section.

were employed (±12°/20 m from centerline compared to ±20°/35 m, as defined as 10% max value). Release height had less of an overall effect, but it changed predictions quite significantly very close to the source. Once again, when a higher deposition velocity was set, the model would have calculated more of the plume deposition with distance, leading to smaller air concentrations downwind.

RIMPUFF reports its predictions in 50 m by 50 m grids, as evident by the shape of the profiles in Fig. 6. The integrated air concentrations that it predicts are fairly similar to the MLCD and ADDAM/CSA-ERM predictions, varying between 10^{-3} s m^{-3} and 10^{-5} s m^{-3}. One of the major differences was that RIMPUFF's predictions remained much more constant, still decreasing, but more slowly as the distance from ground zero increased. RIMPUFF had a lot less flexibility in terms of user defined deposition velocities, and so its sensitivity to v_d could not be investigated. Likewise, sensitivity to release height was not investigated, and runs carried out with different meteorological conditions were fairly similar to one another.

The sensitivity of the different models to input parameters, in terms of general trends for their air concentration predictions, are summarized in Table 7. Although each model has its own particularities, their general sensitivities to each of the input parameters are as follows:

- Stronger, more direct winds tend to result in less lateral dispersion, though the influence on centerline concentration is mixed. The Gaussian plume model in ADDAM/CSA-ERM is the most sensitive to different meteorological inputs;
- Increasing the vertical height of the initial cloud results in slightly lower air concentrations near the source, due to the dilution effect in the vertical. The effects farther afield are fairly small, however; and
- Increasing the deposition velocity means that, in the model calculations, more material will be deposited on the ground and less will stay airborne.

Sensitivity of ground concentration predictions

Predictions for ground concentrations as dilution ratios that result from the deposition of aerosolized material are shown in Figs. 7 to 9. Model to model, predictions can be quite different, but this is primarily due to different levels of flexibility in setting appropriate inputs rather than the underlying method used to calculate deposition. For MLCD and ADDAM/CSA-ERM, predictions are quite close, although MLCD does tend to predict ground concentrations that are lower along the centerline but higher off-centerline. Still, predictions between these two models are generally within an order of magnitude, while they each make predictions that are several orders of magnitude higher than those made by RIMPUFF. More important than the specific model that was used, however, was the deposition velocity that was defined.

For MLCD, ground deposition dilution ratios along the centerline were on the order of 10^{-3} m^{-2} to 10^{-6} m^{-2} with a 250 mm s^{-1} deposition velocity, and 10^{-5} m^{-2} to 10^{-7} m^{-2} with a 3.1 mm s^{-1} deposition velocity. Deposition velocity was by far the most important parameter, and the differences when either meteorological conditions or release height were changed were very small in comparison.

With ADDAM/CSA-ERM, centerline ground deposition dilution ratios were on the order of 10^{-3} m^{-2} to 10^{-6} m^{-2} and 10^{-5} m^{-2} to 10^{-7} m^{-2} for 250 mm s^{-1} and

Table 7. Approximate input sensitivity analysis of predicted integrated air concentrations.

	MLCD	ADDAM / CSA-ERM	RIMPUFF
increasing $\bar{u}$, decreasing σ_θ(average of results from modeling shot 3 to results from modeling shot 1, since meteorological conditions were quite different)			
centerline			
@ 100 m	−15%	−30%	−55%
@ 400 m	+10%	+10%	−50%
increasing release height (average of results from modeling 14 m initial cloud top heights to results from modeling 10 m initial cloud top heights)			
centerline			
@ 100 m	−5%	−30%	—
@ 400 m	+5%	+20%	—
increasing deposition velocity (average of results from modeling with a 250 mms^{-1}deposition velocity to results from modeling with a 3.1 mms^{-1}deposition velocity)			
centerline			
@ 100 m	−50%	−20%	—
@ 400 m	−70%	−70%	—

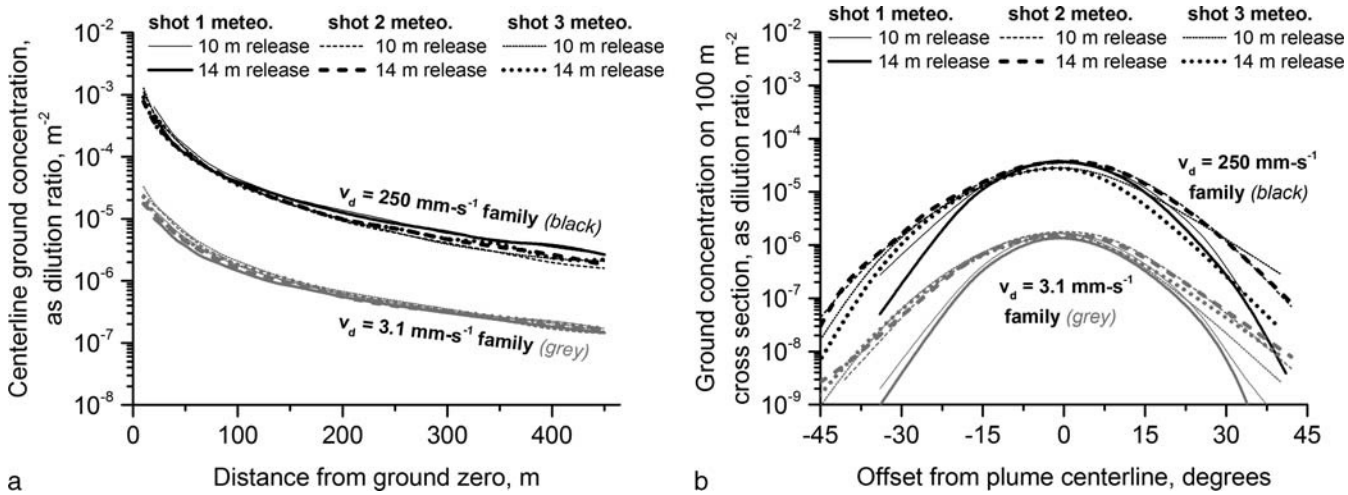

Fig. 7. Ground concentration profiles for MLCD, as dilution ratios: (a) centerline; (b) 100 m cross section.

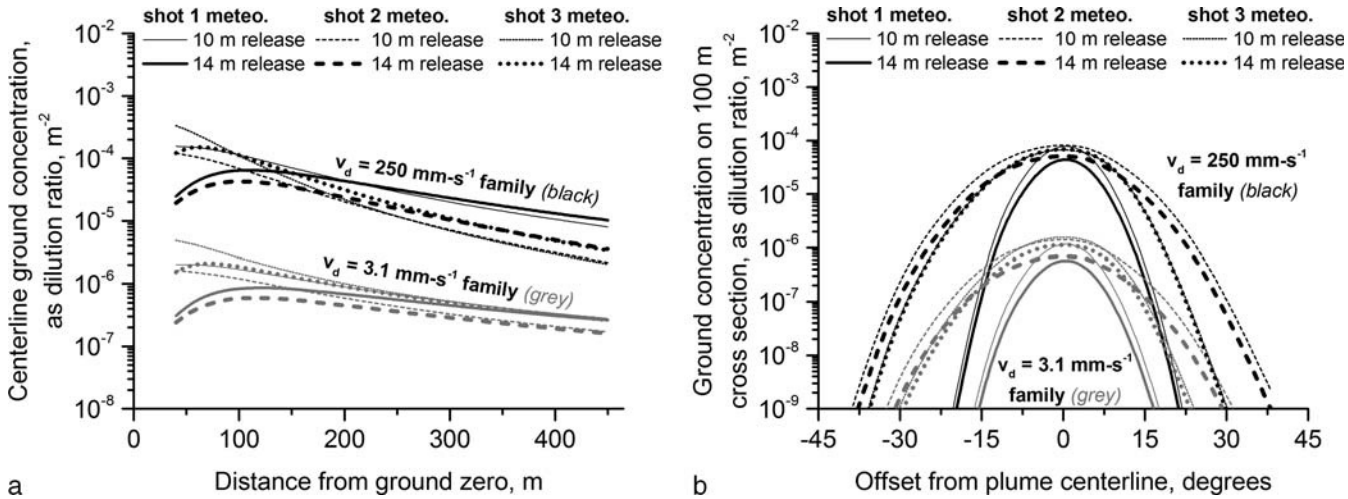

Fig. 8. Ground concentration profiles for ADDAM/CSA-ERM, as dilution ratios: (a) centerline; (b) 100 m cross section.

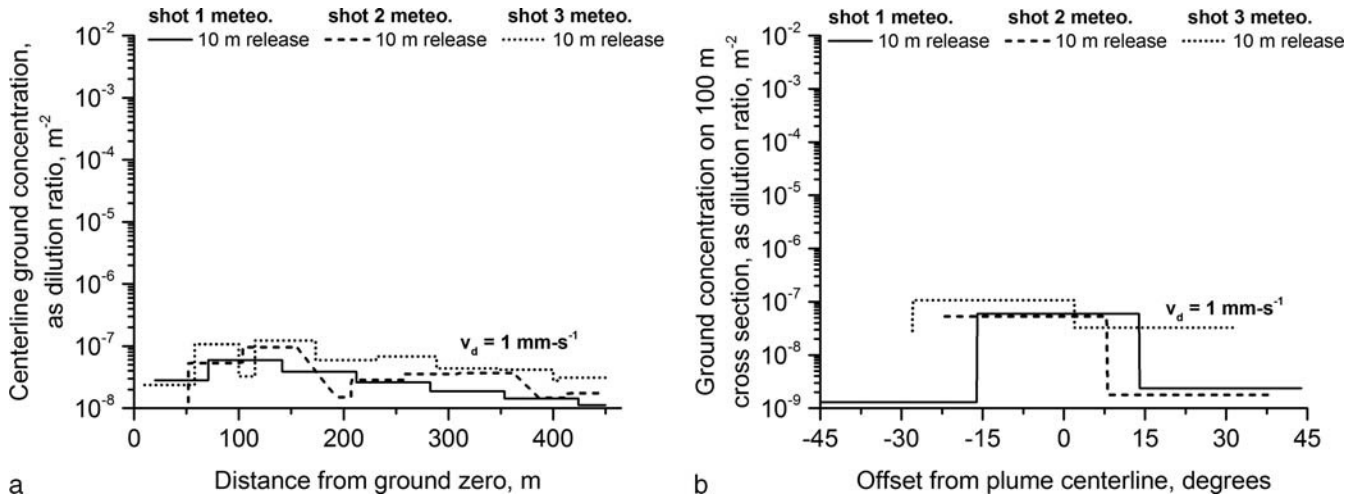

Fig. 9. Ground concentration profiles for RIMPUFF, as dilution ratios: (a) centerline; (b) 100 m cross section.

3.1 mm s^{-1} deposition velocities, respectively. Again, deposition velocity unequivocally had the largest influence on the final predictions, but compared to MLCD, the ADDAM/CSA-ERM predictions were much more strongly influenced by meteorological conditions. Predictions for shot 1 were much narrower as compared to predictions for shot 2 and shot 3. Changing the release height had mixed results on the predictions by ADDAM/CSA-ERM, and overall, they were fairly small compared to other factors.

RIMPUFF was only run under different meteorological conditions and not with different deposition velocities and release heights. The ground deposition dilution ratio predictions were largely between 10^{-7} m^{-2} and 10^{-8} m^{-2} and were somewhat sensitive to wind conditions. Ground concentrations were slightly lower when using the meteorological inputs from shot 1 instead of shot 3. The reason why the deposition predictions are so small with RIMPUFF compared to MLCD and ADDAM/CSA-ERM is largely because RIMPUFF does not have the flexibility to set the deposition velocity any higher than 1 mm s^{-1}. This is a limitation of its design, and although it would be applicable in other situations, the relatively large particle sizes that were generated from the RDDs in the DRDC Suffield trials have deposition velocities that are much faster.

The overall ground deposition sensitivity of each model to the different input parameters is tabulated in Table 8. The key point here is that predictions are extremely sensitive to deposition velocity, and so a good knowledge of the particle size distribution of the released material is essential in order to obtain model predictions that are reasonable to an RDD scenario. This is a consequence of the broad particle size distributions that are generated by RDDs and the sensitive relationship, described in eqn (28), between particle size and the corresponding settling velocity. Besides deposition velocity, generalizations about the sensitivity of the models are that:

- As with air concentration, stronger, more direct winds tend to result in less lateral dispersion and a narrower plume, and once again, ADDAM/CSA-ERM is the most sensitive to such meteorological inputs; and
- The effect of increasing the vertical height of the initial cloud is fairly small overall, especially compared to other effects.

MODEL PREDICTIONS

The previous section showed how sensitive each model is to different input parameters and specifically how meteorological information, initial cloud size definitions, and particle deposition velocity characterizations could affect the predictions made by the models. This section deals with how well model predictions compare with the real observations made during the full-scale RDD trials. Atmospheric dispersion models can provide estimates for how material disperses through the air after it is released; however, in light of the fact that atmospheric transport processes are highly variable and stochastic by nature, it is very difficult for models to exactly reproduce any particular dispersion event. Likewise, small differences in defining the direction of the plume centerline or using simplifying assumptions in the deposition velocity, as underlined in the previous section, can have large effects, and when comparing specific receptor locations can therefore result in fairly large differences between observations and predictions. This can be true even if observations and predictions are qualitatively similar.

Agreement at any particular location within a factor of 10 between dispersion predictions and real observations is

Table 8. Approximate input sensitivity analysis of predicted ground concentrations.

	MLCD	ADDAM / CSA-ERM	RIMPUFF
increasing $\bar{u}$, decreasing σ_θ(average of results from modeling shot 3 to results from modeling shot 1, since meteorological conditions were quite different)			
centerline			
@ 100 m	even	−30%	−45%
@ 400 m	+30%	+100%	−65%
increasing release height (average of results from modeling 14 m initial cloud top heights to results from modeling 10 m initial cloud top heights)			
centerline			
@ 100 m	−10%	−35%	—
@ 400 m	+5%	+20%	—
increasing deposition velocity (average of results from modeling with a 250 mms^{-1}deposition velocity to results from modeling with a 3.1 mms^{-1}deposition velocity)			
centerline			
@ 100 m	+22 times	+60 times	—
@ 400 m	+14 times	+25 times	—

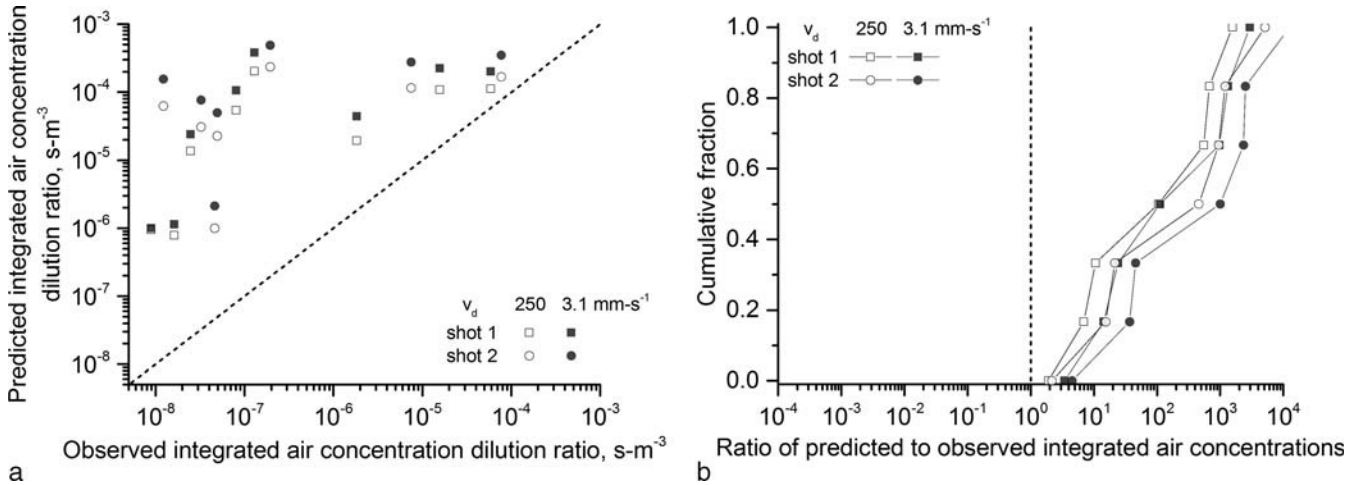

Fig. 10. Comparison of integrated air concentration predictions with observations for MLCD: (a) scatter plot; (b) predicted/observed ratios.

generally acceptable, as long as the predicted contamination profiles qualitatively match the observed profiles. The most amount of confidence is required in areas with higher air and ground concentrations close to the release point (<50 m) and along the plume centerline.

In this section, predictions and observations are compared directly in scatter plots. As well, in order to qualify the number of discrete predictions that are in reasonable agreement with observations, plots of the ratio of predicted over observed concentration, c_{pred}/c_{obs}, versus the observation number are shown. This latter plot is also used in similar model-prediction comparisons by Purves and Parkes (2016) and involves taking ratios of predictions to observations for all available measurement points, sorting them by their magnitude, and then showing the cumulative fraction of measurement points that have prediction to observation ratios below each value.

All comparisons made in this section are for releases with a 10-m cloud top height. Integrated air concentration predictions are compared to observations in Fig. 10 for MLCD, Fig. 11 for ADDAM/CSA-ERM, and Fig. 12 for RIMPUFF. In all cases, the models systematically overpredict air concentration, but near the plume centerline and closer to the release point, which are more important locations, predictions are fairly reasonable. The five largest observations during the field measurements corresponded to position (37.5°N, 100 m), (45°N, 150 m), and (37.5°N, 250 m) for shot 1, and (67.5°N, 100 m) and (75°N, 150 m) for shot 2, and for this cluster, all predictions agreed with observations within a factor of about 30. For measurement points (37.5°N, 100 m) in shot 1 and (67.5°N, 100 m) in shot 2, which were the closest, most central locations, the model predictions agreed with observations within a factor of about 2.

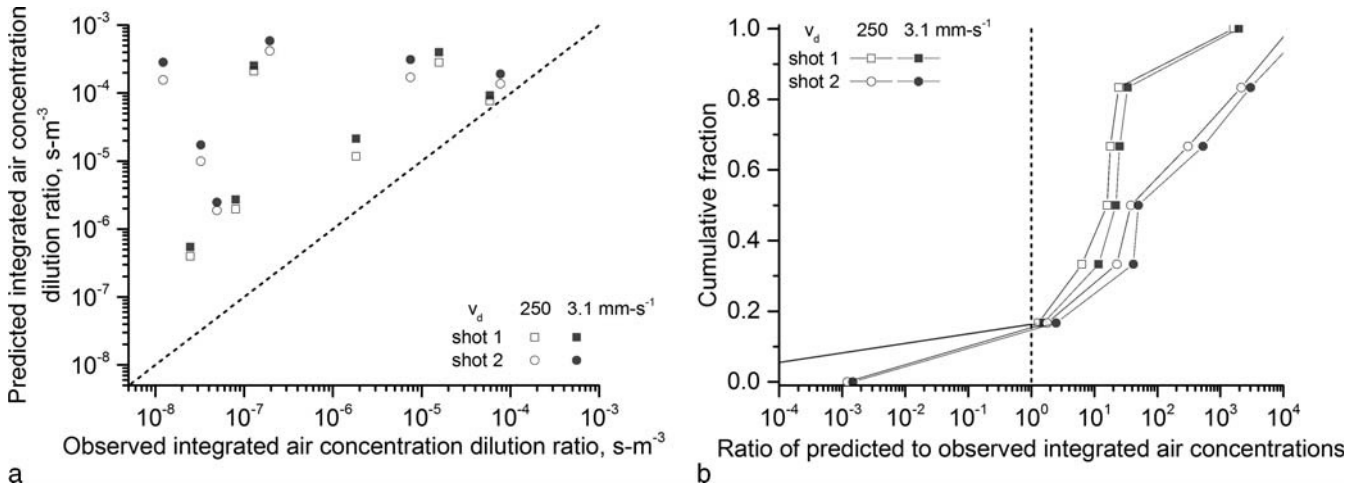

Fig. 11. Comparison of integrated air concentration predictions with observations for ADDAM/CSA-ERM: (a) scatter plot; (b) predicted/observed ratios.

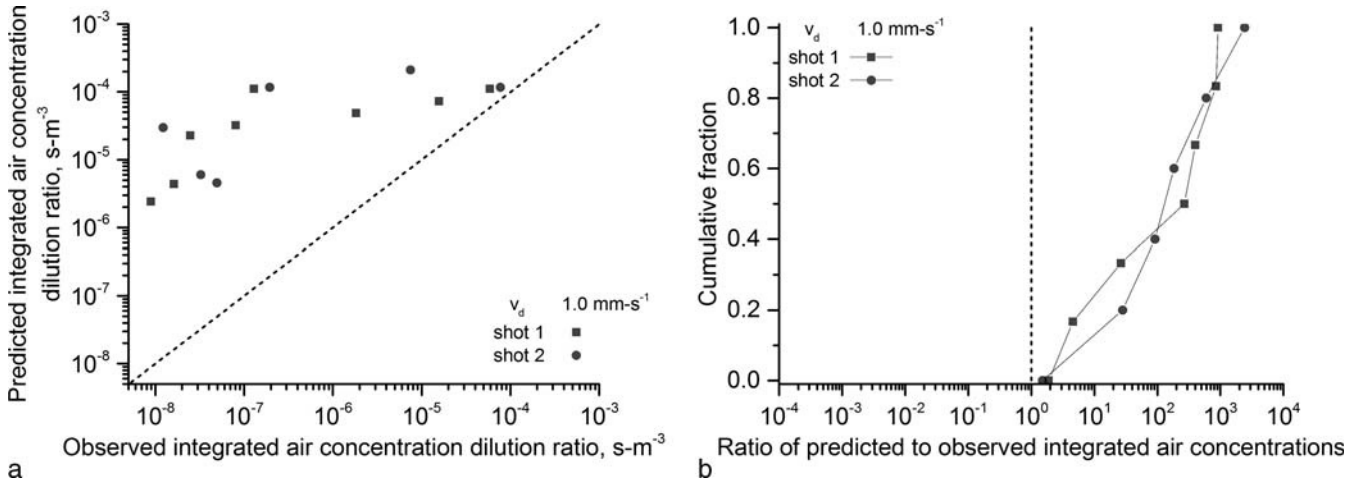

Fig. 12. Comparison of integrated air concentration predictions with observations for RIMPUFF: (a) scatter plot; (b) predicted/observed ratios.

In terms of how each of the different models performed, they all generated fairly similar predictions, and each compared with observations in similar ways. The deposition velocity setting had a fairly small influence on integrated air concentration predictions, although using higher values meant that predictions were slightly smaller and therefore were slightly closer to observations. While agreement was fairly good near the plume centerline, there was very poor agreement, and models significantly overpredicted the integrated air concentration at locations that were at a significant distance from the central path of the radioactive plume.

With the more off-centerline positions, measurements reported air concentrations that were very low, implying a fairly small diameter cloud, with the highest concentration regions missing the different air samplers. Likewise, the lift-off of the radioactive clouds above the ground was observed in the RDD trials. For example, Okada et al. (2016) reported that during shot 1, an air sampler that was elevated 10 m in the air detected the plume, while in a second shot at the same location but at ground level, the air concentration was below detection limits. Dispersion models in general predict plumes that are fairly smooth in shape, as opposed to the heterogeneous, complex, and meandering clouds that are observed in reality.

For ground deposition, the importance of the deposition velocity setting is underlined by examining how model predictions compare to results, as seen in Figs. 13 to 15. Fig. 13, for example, compares MLCD predictions with observations. Different deposition velocities produce predictions that are orders of magnitude different. Although the points are quite scattered in Fig. 13a, predictions that were made with the deposition velocity set to 3.1 mm s^{-1} agree reasonably well with observations. Generally, predictions are within a factor of 100 of observations and, as shown in Fig. 13b, are within a factor of 10 about 60% of the time. However, many of the higher-concentration observations (those closer to the source or along the plume centerline)

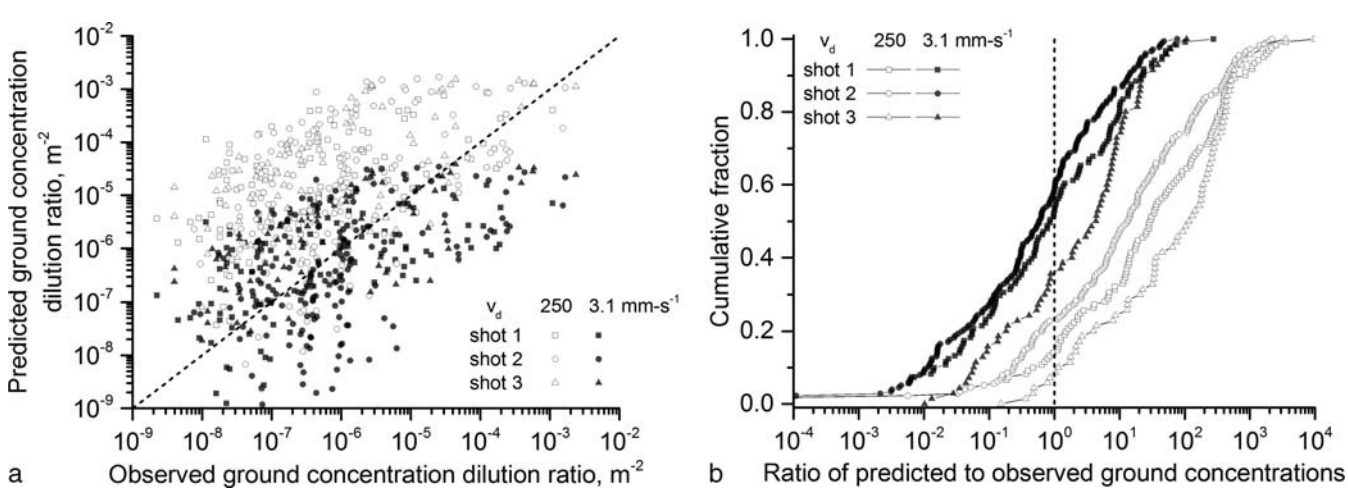

Fig. 13. Comparison of ground concentration predictions with observations for MLCD: (a) scatter plot; (b) predicted/observed ratios.

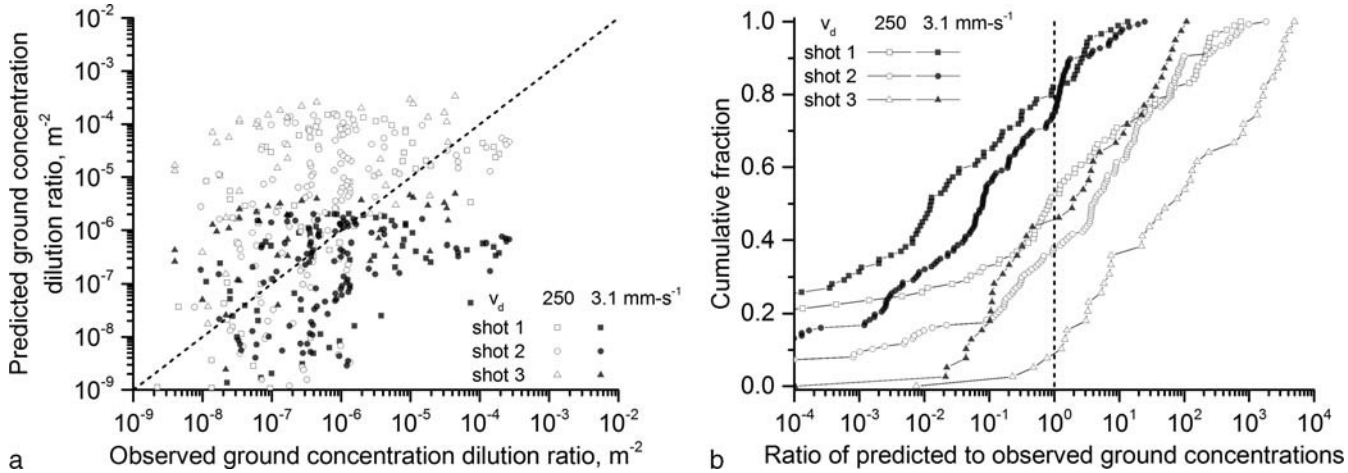

Fig. 14. Comparison of ground concentration predictions with observations for ADDAM/CSA-ERM: (a) scatter plot; (b) predicted/observed ratios.

are significantly under-predicted. In general, predictions made with the deposition velocity set to 250 mm s^{-1} are well above what was observed, but that is mostly due to the fact that MLCD predicted that the contamination profile was wider in the cross wind direction than what was actually observed. Still, predictions were within a factor of 10 of observations 25–40% of the time, and predictions along the plume centerline and closer to the source were much more realistic.

For ADDAM/CSA-ERM, ground deposition predictions are compared to observations in Fig. 14. Once again, the results underline how sensitive predictions are to deposition velocity. Whereas ADDAM/CSA-ERM typically under-predicted ground concentration when the deposition velocity was set to the lower value of 3.1 mm s^{-1}, there were more overpredictions when the deposition velocity was set at 250 mm s^{-1}. Nevertheless, a reasonably large fraction of the predictions were in good agreement, with about 35–50% of predictions within a factor of 10 of the observation value.

Large over-predictions occur with ADDAM/CSA-ERM as well, and for the same reasons: the real contamination profile was narrower than what was predicted by the model, or there was a small mismatch between the real plume direction and that derived from wind measurement. Large underpredictions, on the other hand, generally corresponded to points that were far off-centerline, where the general post-shot background in the vicinity of the tests was still above the near zero values predicted by ADDAM/CSA-ERM. The most important point is that the most representative ground concentration predictions were typically those near the centerline, and those at the highest contamination levels, which are the areas of most interest in the case of disaster planning and emergency response.

With RIMPUFF, ground concentration predictions were significantly underestimated. The model employs deposition velocities that correspond to micron- and submicron-sized particles. Although this would be appropriate for a nuclear power plant-type accident, a deposition velocity of 1.0 mm s^{-1}, the highest value that can

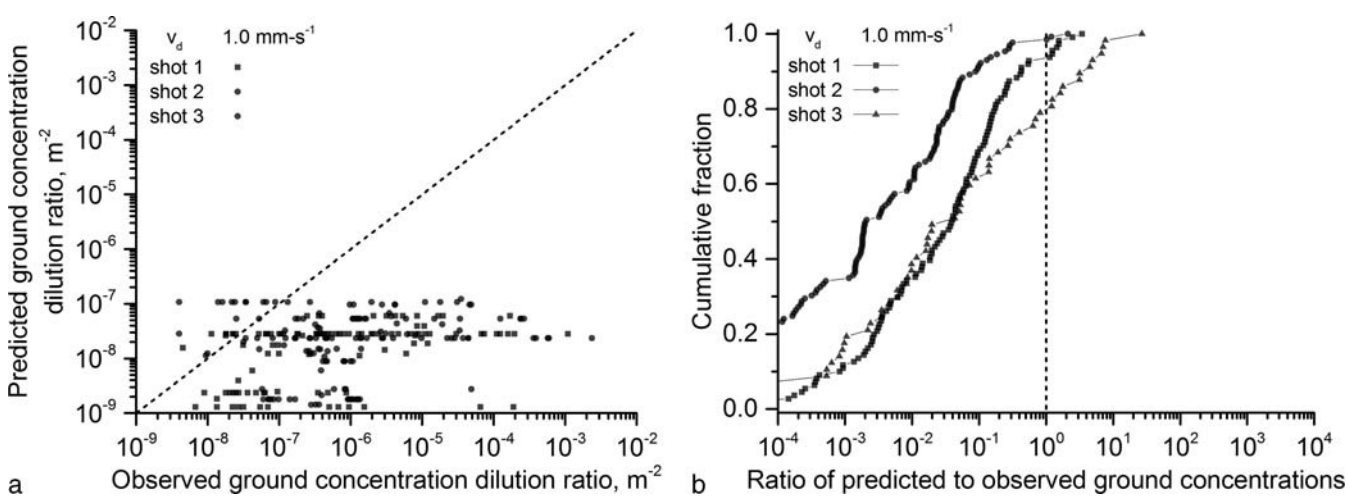

Fig. 15. Comparison of ground concentration predictions with observations for RIMPUFF: (a) scatter plot; (b) predicted/observed ratios.

be set in the model input, cannot adequately represent for an RDD source term where the particle sizes and settling velocities are much larger. The predictions that do match well were typically coincidental, corresponding to low-level contamination, off-centerline points. In the highest contamination areas and along the plume centerline, RIMPUFF predictions were on the order of 10^2 to 10^5 times under-predicted.

CONCLUSION

Atmospheric dispersion models are tools that, in the context of radiological and nuclear safety, are used for safety analysis, disaster planning, and, when required, emergency response. For these purposes, they are meant to give predictions that are reasonable approximations of what may occur during a real incident and therefore are to be used to guide what sort of response would be required. Important metrics for radiological dispersal devices are: (i) the total contaminated area, including the general direction and overall shape of the contamination profile; (ii) the linear extent of contamination downwind; and (iii) the maximum dose rates expected on the ground after the event. These are in addition to health consequence factors, such as the total doses and latent cancer fatality risks to individuals exposed to the radioactive plume emitted by the RDD.

The dispersion models evaluated in this paper can provide estimates for each of these factors, although dose rate-related factors are presented in Part II of this study and in Lebel et al. (2016). This paper has presented how well model predictions compare to the real observations of air and ground concentration made during the full scale RDD trials. All of the atmospheric dispersion models are very complex and have many different parts, and it is unclear if any particular numerical method for calculating dispersion (e.g., Lagrangian particle dispersion vs. Lagrangian puff modeling vs. Gaussian plume modeling) is better or worse than any other in such near-field applications. What is important, however, is how each part of the dispersion models function based on the inputs that are provided to them. This study has attempted to evaluate how important each of those parts are, relative to one another, in order to obtain results that reasonably describe the dispersion that occurs.

Meteorological inputs, including wind speed, direction, variability, and atmospheric stability, establish the overall direction of the plume and also establish how wide or narrow the plume will extend crosswind to the centerline. Stronger, more direct winds, of course, yield faster moving clouds and narrower contamination profiles on the ground. Overall, however, meteorological inputs are of medium importance. The direction of the plume is very important, but near the source and near the plume centerline, where the highest concentrations are observed, different meteorological inputs do not have a very large effect on predictions.

Release inputs including the initial cloud top height and the shape of the cloud directly after the detonation of an RDD influences ground concentrations near the source, since a higher cloud will mean that less will initially deposit. Compared to other inputs, however, this factor has a small effect overall.

Source term characterization, including the particle size and deposition velocity of the material released by the RDD, has the largest influence on predictions. With higher values for deposition velocity, the models calculated more plume depletion, resulting in lower downwind air concentrations. Most importantly, however, the large range of possible particle sizes, plus the strong relationship between particle size and deposition velocity, meant that ground concentration predictions could be orders of magnitude different.

For integrated air concentration, all three models performed reasonably well in higher concentration areas near the plume centerline and close to the source. For ground concentration, it was much more important to have a good understanding of what the particle size and deposition velocity would be. Results were quite reasonable when the deposition velocity values closely matched with those expected from source characterization experiments. When deposition velocity could not be well characterized, however, the models produced results that were very different from the observations.

This is an important lesson since, when planning for a real RDD event, the particle sizes that would be produced would not be known in advance. RDDs dispersing a liquid ^{99m}Te source, a metallic ^{60}Co source, and a ceramic ^{137}Cs source could all produce drastically different particle sizes based on the target's material properties, as well as the design of the explosive device (Harper et al. 2007). In emergency planning, the information that would be provided by an atmospheric dispersion model could be extremely valuable, but in order to obtain model predictions that are reasonable, the inputs provided to the model must also be reasonable. Reasonable inputs, in turn, require realistic assessments of the threat and a good understanding of the physics that go into explosively dispersing the radiological materials.

Acknowledgments—The authors are greatly appreciative to all those involved in the DRDC Suffield full scale RDD experiments and their tremendous efforts. The authors would also like to acknowledge Dmytro Trybushnyi of the Karlsruhe Institute of technology for his help and support for the RIMPUFF modeling effort. This study was supported in part by the Canadian Safety and Security Program under project CSSP-2013-CD-1131 and by the Canadian Nuclear Laboratories Nuclear Safety and Security Program under project RDC-1.2.1-1-5929.

REFERENCES

Arya SP. Air pollution meteorology and dispersion. Oxford: Oxford University Press; 1999.

Canadian Standards Association. Guidelines for calculating radiation doses to the public from a release of airborne radioactive material under hypothetical accident conditions in nuclear reactors. CSA N288.9-M91; 1991.

Cao X, Roy G, Brousseau P, Erhardt L, Andrews W. A cloud rise model for dust and soot from high explosive detonations. Propellants Explos Pyrotech 36:303–309; 2011. DOI: 10.1002/prep.200900033.

D'Amours R, Malo A, Flesch T, Wilson J, Gauthier J-P, Servranckx R. The Canadian Meteorological Centre's Atmospheric Transport and Dispersion Modelling Suite. Atmosphere–Ocean 53:176–199; 2015. DOI: 10.1080/07055900.2014.1000260.

Ehrhardt J, Weis A. RODOS: decision support system for off-site nuclear emergency management in Europe. Brussels, Belgium: European Commission; Report EUR-19144-EN; 2000.

Erhardt L, Lebel L, Korpach E, Berg R, Inrig E, Liu C, Watson I, Quayle D. Deposition measurements from the full-scale radiological dispersal device field trials. Health Phys 110(5):442–457; 2016.

Flesch TK, Wilson JD, Crenna BP. MLCD: a short-range atmospheric dispersion model for emergency response. Edmonton, Alberta: University of Alberta; Contract report to Environment Canada; 2002.

Green AR, Erhardt L, Lebel L, Duke J, Quayle D, Jones T, White D. Overview of the full scale radiological dispersal device field trials. Health Phys 110(5):403–417; 2016.

Hanna SR, Briggs GA, Deardorff J, Egan BA, Gifford FA, Pasquill F. AMS workshop on stability classification schemes and sigma curves—summary of recommendations. Bull Am Meteorological Soc 58:1305–1309; 1977.

Harper FT, Mussolino SV, Wente WB. Realistic radiological dispersal device hazard boundaries and ramifications for early consequence management decisions. Health Phys 93:1–16; 2007.

Hinds WC. Aerosol technology: properties, behaviour, and measurement of airborne particles. New York: Wiley-Interscience; 1999.

Hoe S, McGinnity P, Charnock T, Gering F, Jacobsen LHS, Sorensen JH, Andersson K, Astrup P. ARGOS decision support system for emergency management. In: Proceedings of the 12th International Congress of the International Radiation Protection Association. Buenos Aires, Argentina: IRPA; 2009.

Kerschgens MJ, Suer H. Energetic feedback between urban climate and diffusion of atmospheric pollutants. In: Proceedings of the 1st International Symposium on Environmental Meteorology. Dordrecht, The Netherlands: Kluwer Academic Publishers; 1988.

Korpach E, Berg R, Erhardt L, Lebel L, Liu C. Real time in-situ gamma radiation measurements of the plume evolution from the full-scale radiological dispersal device field trials. Health Phys 110(5):427–435; 2016.

Lebel LS. Aerosolization and soil entrainment in explosive fireballs. Royal Military College of Canada; 2012. Dissertation.

Lebel LS, Brousseau P, Erhardt L, Andrews WS. Entrainment of powders and soils into explosive fireballs. Internat J Energetic Materials Chem Propulsion 10:351–364; 2012. DOI: 10.1615/IntJEnergeticMaterialsChemProp.2012005239.

Lebel LS, Bourgouin P, Chouhan S, Ek N, Korolevych V, Malo A, Bensimon D, Erhardt L. Radiation modeling and finite cloud effects for atmospheric dispersion calculations in near-field applications: modeling of the full scale RDD experiments with operational models in Canada part II. Health Phys 110(5):518–525; 2016.

Okada CE, Keillor M, Kernan W, Kirkham R, Sorom RD, Van Etten DM. Measuring concentrations of particulate ^{140}La in the air. Health Phys 110(5):418–426; 2016.

Purves M, Parkes D. Validation of the DIFFAL, HPAC and HotSpot Dispersion Models Using the Full-Scale Radiological Dispersal Device (FSRDD) Field Trials Witness Plate Deposition Dataset. Health Phys 110(5):481–490; 2016.

Rodean HC. Stochastic Lagrangian models of turbulent diffusion. Meteological Monographs 26:1–84; 1996. DOI: 10.1175/0065-9401-26.48.1.

Scheier NW. ADDAM version 1.4 theory manual. Chalk River, Canada: Atomic Energy of Canada; Report 153-11090-COG-005; 2009.

Taylor GI. Diffusion by continuous movements. Proc London Math Soc 20:196–211; 1921.

Thykier-Nielsen S, Deme S, Mikkelsen T. Description of the atmospheric dispersion module RIMPUFF. Roskilde, Denmark: RODOS Consortium; Report RODOD(WG2)-TM(98)-02; 1999.

Wilson JD, Ferrandino FJ, Thurtell GW. A relationship between deposition velocity and trajectory reflection probability for use in stochastic Lagrangian dispersion models. Agricultural and Forest Meteorology 47:139–154; 1989. DOI: 10.1016/0168-1923(89)90092-0.

Wilson JD, Flesch TK. An idealized mean wind profile for the atmospheric boundary layer. Boundary-Layer Meteorol 110(5):281–299; 2004. DOI: 10.1023/A:1026044025803.

■■